

Stepwise Ordering of Imidazolium-Based Cationic Surfactants during Cooling-Induced Crystallization

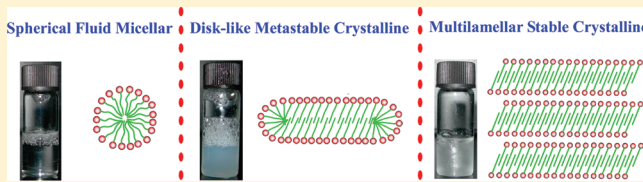
Fu-Gen Wu,[†] Ji-Sheng Yu,[†] Shu-Feng Sun,[‡] Hai-Yuan Sun,[†] Jun-Jie Luo,[†] and Zhi-Wu Yu*,[†]

[†]Key Laboratory of Bioorganic Phosphorous Chemistry and Chemical Biology, Ministry of Education, Department of Chemistry, Tsinghua University, Beijing 100084, PR China

[‡]Lab of Bio-imaging, Core Facilities, Institute of Biophysics, Chinese Academy of Sciences, Beijing 100101, PR China

Supporting Information

ABSTRACT: Surfactants bearing imidazolium cations represent a new class of building blocks in molecular self-assembly. These imidazolium-based cationic surfactants can exhibit various morphologies during phase transformations. In this work, we studied the self-assembly and phase behavior of 1-hexadecyl-3-methylimidazolium chloride ($C_{16}\text{mimCl}$) aqueous dispersions (0.5–10 wt %) by using isothermal titration calorimetry, differential scanning calorimetry, synchrotron small- and wide-angle X-ray scattering, freeze-fracture electron microscopy, optical microscopy, electrical conductance, and Fourier transform infrared spectroscopy. It was found that $C_{16}\text{mimCl}$ in aqueous solutions can form two different crystalline phases. At higher $C_{16}\text{mimCl}$ concentrations (>6 wt %), the initial spherical micelles convert directly to the stable crystalline phase upon cooling. At lower concentrations (0.5 or 1 wt %), the micelles first convert to a metastable crystalline phase upon cooling and then transform to the stable crystalline phase upon further incubation at low temperature. The electrical conductance measurement reveals that the two crystalline phases have similar surface charge densities and surface curvatures. Besides, the microscopic and spectroscopic investigations of the two crystalline phases suggest that the metastable crystalline phase has preassembled morphology and a preordered submolecular packing state that contribute to the final stable crystalline structure. The formation of a preordered structure prior to the final crystalline state deepens our understanding of the crystallization mechanisms of common surfactants and amphiphilic ionic liquids and should thus be widely recognized and explored.



1. INTRODUCTION

Crystal polymorphism, the phenomenon of a substance crystallizing with two or more crystalline structures, is widely observed in inorganic materials,^{1,2} simple organic compounds,^{3–5} amphiphilic molecules,^{6–11} and polymers.^{12–14} As stated by Ostwald's Rule of Stages,¹⁵ the metastable crystal form should appear first during crystallization from solution, and it should then transform into the stable form. The occurrence of metastable intermediate states en route to the most stable final structure of a substance not only changes the crystallization process but also may result in different structures and/or morphologies of the substance.¹⁶ The occurrence of metastable crystalline phases represents a preordering process toward the final stable crystalline structures. Such stepwise ordering of molecules from the initial fluid or fused state to the final ordered crystalline state is a fascinating topic. There have been discussions on the preordering in the crystallization of polymers.^{17–19} This preordering process may be related to the difficulty in the movement of the polymer segments or side groups. For self-assembled aggregates composed of medium-molecular-weight amphiphiles, stepwise ordering may also occur toward their crystalline states to fulfill the specific geometrical or packing/hydration requirements during the formation of the intermediate morphologies or structures. A multiangle investigation (macroscopic, microscopic, and even

submolecular-level) on the preordering of amphiphiles in aqueous solutions would facilitate an in-depth understanding of their crystallization processes. Different from the crystallization of simple organic compounds or salts from supersaturated solutions, the crystallization process of amphiphiles in aqueous solutions is special because they have preassembled or prealigned into various ordered structures prior to crystallization. Hence, some new insights could be obtained for such preordering phenomena by exploring the formation and transformation mechanisms of the metastable crystalline phase of amphiphiles. Besides, because of the lack of metastable crystalline phases with lifetimes long enough to be investigated, the physics of the metastable crystalline phase in aqueous solutions has not been well explored. It is therefore essential to find a suitable amphiphilic system with a long-lived metastable crystalline phase en route to the final stable crystalline phase. To find such a system, we will pay attention to the surfactants bearing imidazolium cations.

Molecules with imidazolium cations are receiving increasing interest from researchers in fields such as ionic liquids (ILs), colloid and interface science, and supramolecular chemistry.

Received: February 20, 2012

Revised: April 23, 2012

Published: April 26, 2012



The various physiochemical properties of neat imidazolium-based ILs^{20–25} and their application as solvents in assembling amphiphiles have been extensively studied.^{26–32} Another important classification is imidazolium-based molecules with long alkyl chains (i.e., amphiphilic ionic liquids or AILs). These hydrophobic long alkyl chains endow these molecules with amphiphilic characteristics, and such molecules are actually one kind of cationic surfactant. When dispersed in water, these imidazolium-based surfactants can self-assemble into well-organized structures in various mesophases. In fact, because these imidazolium-based cationic surfactants can be used as important building blocks in self-assembly, the aggregation behaviors of these imidazolium-based surfactants in aqueous solution have been extensively studied.^{33–46} However, studies of the phase behaviors of these imidazolium-based surfactants in aqueous solutions are very rare,^{47,48} and a detailed submolecular-level understanding of the phase-transition mechanisms of the imidazolium-based surfactants remains largely unknown.

In this work, we selected 1-hexadecyl-3-methylimidazolium chloride ($C_{16}\text{mimCl}$, Figure 1) to study the self-assembly and

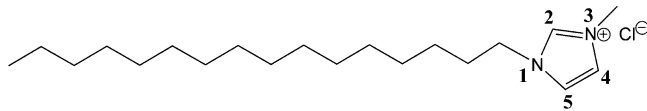


Figure 1. Molecular structure of $C_{16}\text{mimCl}$.

phase behavior of its aqueous dispersions by using isothermal titration calorimetry (ITC), differential scanning calorimetry (DSC), optical microscopy, synchrotron small- and wide-angle X-ray scatterings (SAXS and WAXS), freeze-fracture electron microscopy (FFEM), Fourier transform infrared (FTIR) spectroscopy, and electrical conductance measurements. It was found that at low concentrations (e.g., 1 wt %) $C_{16}\text{mimCl}$ can form a long-lived metastable crystalline phase upon cooling from the fluid micellar phase in aqueous solution, which eventually converts to the final stable crystalline phase upon prolonged low-temperature incubation. The long-lived characteristic of the metastable crystalline phase enables us to investigate the nature of the metastable phase and its formation and transformation properties.

2. EXPERIMENTAL SECTION

2.1. Sample Preparation. 1-Hexadecyl-3-methylimidazolium chloride ($C_{16}\text{mimCl}$) monohydrate (98%) was purchased from

Acros Organics. To prepare the $C_{16}\text{mimCl}$ aqueous dispersions, doubly deionized water with a resistivity of 18.2 MΩ·cm was used. Samples with $C_{16}\text{mimCl}$ concentrations of 0.5–10 wt % are all clear solutions at room temperature.

2.2. ITC. ITC measurements were performed with a VP-ITC calorimeter (MicroCal) at 25 °C. The reaction cell ($V = 1.46 \text{ mL}$) was filled with degassed doubly deionized water (18.2 MΩ·cm). The syringe (280 μL) was loaded with a 10 mM $C_{16}\text{mimCl}$ solution, which was injected into the reaction cell in 28 steps of 10 μL aliquots each, and the heat flow was measured. During the titration, the stirring speed was 307 rpm. The duration of each injection was 20 s, and the equilibration time between consecutive injections was 5 min. Calorimetric data analysis was carried out using Origin 7.0 software (MicroCal).

2.3. DSC. Thermal data were obtained with a DSC821^e differential scanning calorimeter equipped with an HSS7 high-sensitivity sensor (Mettler-Toledo Co., Switzerland). For each measurement, about 60 μL of the $C_{16}\text{mimCl}$ solution was sealed in a 100 μL aluminum pan.

2.4. Synchrotron X-ray Diffraction. SAXS and WAXS experiments were performed at beamline 1W2A of the Beijing Synchrotron Radiation Facility (BSRF) ($\lambda = 1.54 \text{ \AA}$). A standard silver behenate sample was used for the calibration of diffraction spacings. X-ray scattering intensity patterns were recorded during 60–600 s exposure of the samples to the synchrotron beam. To obtain the SAXS data, we fixed the sample-to-detector distance at 1662.0 mm. To obtain the WAXS data (and partial SAXS data), we fixed the sample-to-detector distance at 299.5 mm. A Linkam thermal stage (Linkam Scientific Instruments, United Kingdom) was used for temperature control ($\pm 0.1 \text{ }^{\circ}\text{C}$). The X-ray powder diffraction intensity data were analyzed using the Fit2D program.

2.5. FFEM. A freeze-fracture electron microscopy (FFEM) technique was used to characterize the morphology of the 1 wt % $C_{16}\text{mimCl}$ –H₂O sample after incubation at 0 °C for 5 min. The samples and tools used for sample manipulation were equilibrated at the desired temperature for 3 min. A small amount of the suspension was sandwiched between two copper plates and manually plunged into liquid nitrogen. The freeze-fracture procedure was carried out in a Balzers BAF 400D freeze-fracture apparatus. Fractured surfaces were shadowed with platinum/carbon. Platinum and carbon evaporation was carried out at 45 and 90°, respectively. Replicas were floated on methanol–chloroform (1/3 v/v) mixed solvents to remove organic materials. Images were then recorded with a JEOL 2010 transmission electron microscope (JEOL Ltd., Tokyo, Japan).

2.6. Optical Microscopy. An inverted Olympus IX71 microscope (Olympus Optical, Tokyo, Japan) was used to observe the appearance of the 1 wt % $C_{16}\text{mimCl}$ –H₂O sample that had been incubated at ~ 3 °C for more than 6 h. A drop of the sample at ~ 3 °C was spread on the surface of a glass slide that was precooled to ~ 0 °C. Pictures were quickly taken to avoid the change in temperature.

2.7. Electrical Conductance Measurements. Measurements of electrical conductance, κ , were carried out on a conductivity meter

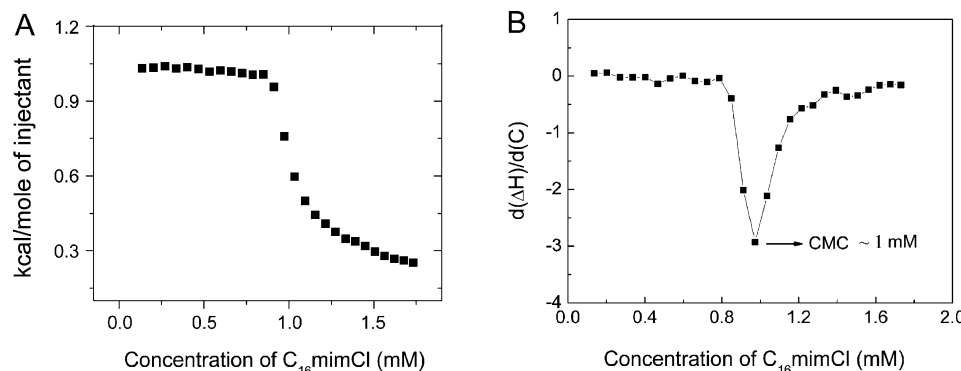


Figure 2. ITC results for the determination of the cmc value of $C_{16}\text{mimCl}$ at 25 °C when a series of 10 mM $C_{16}\text{mimCl}$ solutions (10 μL each) were injected into H₂O. (A) Integrated heat per injection. (B) First derivative of the data in A.

(model DDSJ-308A, Shanghai Leici Instrument Inc., Shanghai, China). The 1 wt % $C_{16}\text{mimCl}-\text{H}_2\text{O}$ sample at 25 °C in a 10 mL tube was quickly transferred to a thermostated water bath preset to the desired temperature of 3 °C.

2.8. FTIR Spectroscopy. FTIR spectra were recorded using a Nicolet 5700 Fourier transform infrared spectrometer with a DTGS detector in the range of 4000–900 cm⁻¹ with a spectral resolution of 2 cm⁻¹ and a zero filling factor of 2. Sample solutions were placed between a pair of CaF₂ windows separated by a 50 μm (for 1 wt % $C_{16}\text{mimCl}-\text{H}_2\text{O}$) or 500 μm (for 1 wt % $C_{16}\text{mimCl}-\text{D}_2\text{O}$) Teflon spacer. A piece of Parafilm was used to wrap the surroundings of the two CaF₂ windows, which were then mounted on a Linkam heating–cooling stage for temperature control (± 0.1 °C). Thirty-two scans were carried out for each spectrum.

3. RESULTS AND DISCUSSION

3.1. ITC and DSC. ITC was used to determine the cmc value of $C_{16}\text{mimCl}$ aqueous dispersions at 25 °C. The ITC results are given in Figure 2 (The ITC titration curve is given in Figure S1 in the Supporting Information.) The thus-obtained cmc value and the micelle dissociation enthalpy are ~ 1 mM (or ~ 0.034 wt %) and 4.3 kJ/mol, respectively. The cmc value suggests that all samples with a concentration of 0.5–10 wt % can form micelles at room temperature.

Next, we employed the DSC technique to examine the phase behavior of the $C_{16}\text{mimCl}-\text{H}_2\text{O}$ mixtures during heating at $C_{16}\text{mimCl}$ concentrations of 0.5–10 wt % (Figure S2 in the Supporting Information). The samples were first cooled to –5 at 0.5 °C/min and then immediately heated from –5 to 25 °C at 0.5 °C/min. During cooling, a single exothermic peak occurs below 2 °C for the 1 wt % sample and below 5 °C for the 10 wt % sample (data not shown). Because of the supercooling effect of water, no ice formed at this temperature. However, upon heating, we can see from Figure S2 that for the 10, 7.5, and 6 wt % samples the DSC curves exhibit almost exclusively one peak centered at ~ 14 °C. The transition enthalpies are almost the same (~ 55 kJ/mol) for these three samples. At 5 wt %, a tiny peak centered at 10.5 °C occurs, and this peak grows as the concentration of $C_{16}\text{mimCl}$ decreases. At 1 and 0.5 wt %, the DSC curves exhibit almost exclusively one peak centered at 10.9 and 8.8 °C, respectively. The transition enthalpies are almost identical (~ 45 kJ/mol) for the two samples. These DSC results may indicate the presence of two crystalline states in the 0.5–10 wt % $C_{16}\text{mimCl}$ samples: one is the metastable crystalline phase with a lower transition temperature (10.9 or 8.8 °C) and a smaller transition enthalpy (~ 45 kJ/mol), and the other is the stable crystalline phase with a higher transition temperature (~ 14 °C) and a higher transition enthalpy (~ 55 kJ/mol). For the 1 and 10 wt % samples, the large differences in the phase-transition onset temperatures during cooling and heating, namely, transition hysteresis, indicate that the formations of the two crystalline phases are difficult (data not shown).

For the 1 wt % $C_{16}\text{mimCl}-\text{H}_2\text{O}$ sample, we have also carried out additional DSC experiments where the samples before measurements were first cooled to –5 at 5 °C/min to ensure the formation of the metastable crystalline phase. They were then heated to 3 at 10 °C/min followed by incubation at 3 °C for various periods. This procedure avoided ice formation and allowed us to monitor the transformation of the metastable crystalline phase to a more stable one. The DSC curves after the thermal treatments are shown in Figure 3. We can see that incubations at 3 °C for 0, 30, and 40 min all give only one peak centered at ~ 11 °C. The transition enthalpies are all ~ 45 kJ/mol.

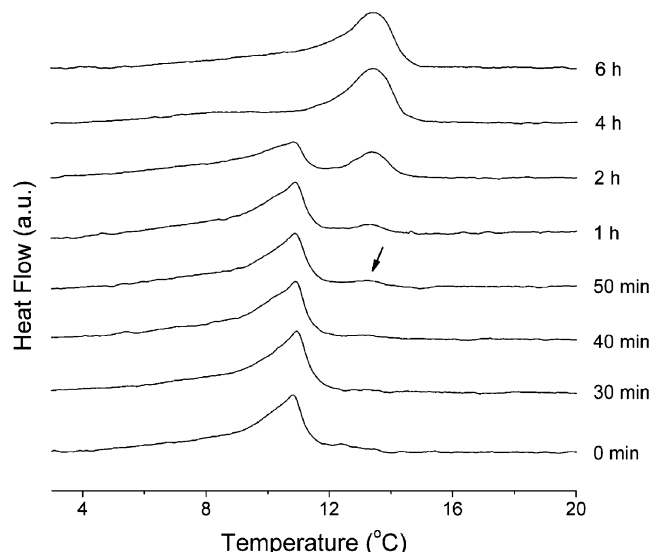


Figure 3. DSC heating results of the $C_{16}\text{mimCl}-\text{H}_2\text{O}$ (1 wt %) system after incubation at 3 °C for different periods of time.

mol. After incubation at 3 °C for 50 min, a small peak at ~ 13 °C occurs, and this peak increases as the incubation time increases. After incubation at 3 °C for 6 h, the sample shows exclusively one peak at ~ 13.5 °C with a transition enthalpy of ~ 54 kJ/mol. The presence of the second peak with a higher transition temperature and a larger transition enthalpy indicates the conversion of the metastable crystalline phase to the stable crystalline phase during the 3 °C incubation.

3.2. SAXS and WAXS. The SAXS data of the 1, 3, and 10 wt % $C_{16}\text{mimCl}-\text{H}_2\text{O}$ samples at 25 °C all exhibit only one broad, diffuse peak at $q_m = \sim 0.55$, ~ 0.61 , and ~ 0.80 nm⁻¹, respectively (Supporting Information, Figure S3). These are intermicelle interference peaks, from which we can calculate the correlation lengths (ξ_C) of pair distribution functions of micelles using the equation $q_m = 2\pi/\xi_C$.⁶ The thus-obtained ξ_C values for the three samples are ~ 11.4 , ~ 10.3 , and ~ 7.9 nm, respectively. The data show that the intermicellar distance of the $C_{16}\text{mimCl}$ sample decreases as the concentration increases.

The assignment of the SAXS peaks at 0.55–0.80 nm⁻¹ is consistent with the literature for a similar chloride-containing system, cetylpyridinium chloride (CPC)–water.⁶ Besides, the attribution of the peaks at 0.55–0.80 nm⁻¹ to the intermicelle interference peaks is reasonable because the peak assigned to the form factor of individual micelles in chloride-bearing surfactants is very weak.⁴⁹ Moreover, for $C_{16}\text{mimCl}$ concentrations of 1–10 wt %, the sizes of the micelles do not depend on concentration as evidenced by our DLS data (not shown) and the corresponding FFEM images. If the peak comes from the form factor of individual micelles, then the shift in peak position during the increase in the surfactant concentration indicates that the micelle size will gradually decrease with increasing surfactant concentration. This is not true for our present spherical micellar system.

To identify the phase state of the micelles at 25 °C, we collected WAXS data for the 1 and 10 wt % $C_{16}\text{mimCl}-\text{H}_2\text{O}$ samples (see Supporting Information, Figure S4). The upshifts of the two curves at $q > 11$ nm⁻¹ result from the presence of a very big, broad peak at higher q values (usually at $q_m = 19$ –20 nm⁻¹ at 0–25 °C) due to the oxygen–oxygen spacing in water.⁵⁰ Although the WAXS peak for the more dilute 1 wt % sample is very weak (Figure S4A), we can observe a very diffuse

peak at $q_m = \sim 14 \text{ nm}^{-1}$ for the more concentrated 10 wt % sample (Figure S4B). From this peak, we can obtain $d = 2\pi/q_m = 0.45 \text{ nm}$. This d value can reflect the packing tightness of the hydrocarbon chains of the surfactant tails because a single, broad diffraction band at 0.44–0.46 nm arises from disordered or melted chains^{51,52} and the result indicates that the sample at 25 °C is in a fluid state. Hence, the SAXS result in Figure S3 and the WAXS result in Figure S4 jointly show that the 10 wt % sample at 25 °C is in the fluid micellar phase. Figure 4 gives the

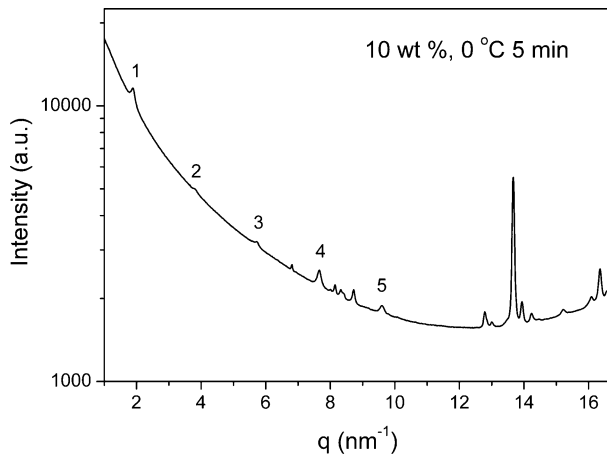


Figure 4. XRD result of the 10 wt % $\text{C}_{16}\text{mimCl}-\text{H}_2\text{O}$ sample after incubation at 0 °C for 5 min.

SAXS (the left part of the curve) and WAXS (the right part of the curve) results for the 10 wt % sample after incubation at 0 °C for 5 min. The periodic Bragg peaks (marked with numbers) in a ratio of 1:2:3:4:5 indicates that the sample is multilamellar, and the occurrence of a number of peaks mainly residing in the wide-angle region ($q > 12 \text{ nm}^{-1}$) proves that the sample is in the crystalline phase. From the periodical Bragg peaks, we can obtain the repeat distances (the d values) using the equation $d = 2\pi/q$. The thus-obtained average d value is 3.2 nm. Because the bilayer thickness (3.2 nm) is smaller than the sum of two fully stretched $\text{C}_{16}\text{mimCl}$ molecules (~5 nm, derived by MM2 force field simulation in the absence of the Cl^- counterion), we may expect that the alkyl chains in this

lamellar crystalline phase are interdigitated and/or tilted. However, on the basis of our present X-ray scattering data we are not able to determine if the layers are tilted or interdigitated because a tilted or interdigitated layer can give the same repeat distance.⁴⁶ The data mean that the 10 wt % sample at 0 °C forms multilamellar crystalline phase. Thus, the corresponding endothermic DSC peak for the 10 wt % sample as shown in Figure S2 is a transition from the multilamellar crystalline phase to the fluid micellar phase.

Figure 5 gives the WAXS results of the two crystalline phases of the 1 wt % sample. When the sample is cooled from 25 °C (in the fluid phase) to 0 °C, several peaks occur after 5 min of incubation (Figure 5A), indicating the formation of an orderly packed crystalline phase. After further incubation at 3 °C for 6 h, a different scattering pattern with more sharp peaks can be observed (Figure 5B), suggesting the formation of a more orderly packed crystalline phase. By combining these results with our above DSC data for the 1 wt % sample (Figure 3), we conclude that the sample after incubation at 0 °C for 5 min is a metastable crystalline phase whereas the sample after incubations at 0 °C for 5 min and 3 °C for 6 h is a stable multilamellar crystalline phase.

3.3. Photographs, FFEM, and Optical Microscopy.

Shown in Figure 6 are photographs of the 10 and 1 wt %

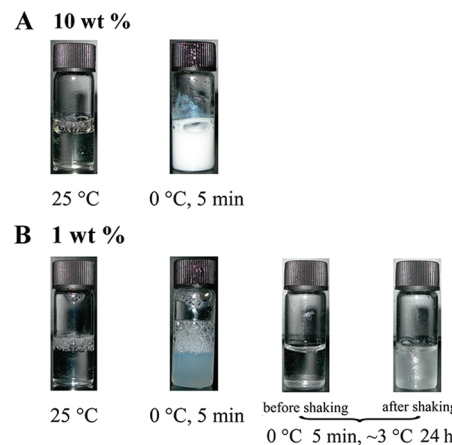


Figure 6. Photographs of the (A) 10 wt % and (B) 1 wt % $\text{C}_{16}\text{mimCl}-\text{H}_2\text{O}$ samples.

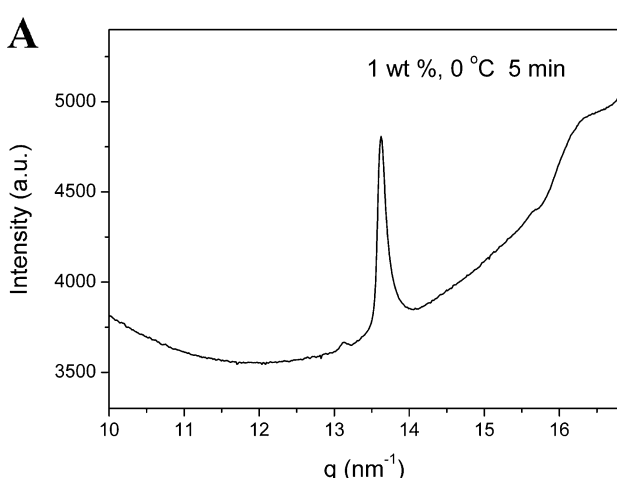
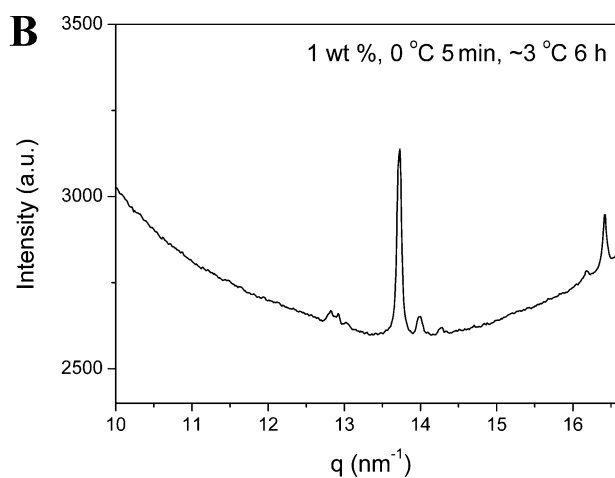


Figure 5. WAXS results of the 1 wt % $\text{C}_{16}\text{mimCl}-\text{H}_2\text{O}$ sample (A) after incubation at 0 °C for 5 min and (B) after incubation at 0 °C for 5 min and ~3 °C for 6 h.



$C_{16}\text{mimCl}-\text{H}_2\text{O}$ samples. The two samples at 25 °C are both clear solutions, consistent with the physical appearance of isotropic micellar structures. The FFEM results reveal that 10–20 nm spherical micelles predominate in these two samples (Figure 7A,B). After cooling to 0 °C, the 10 wt % sample

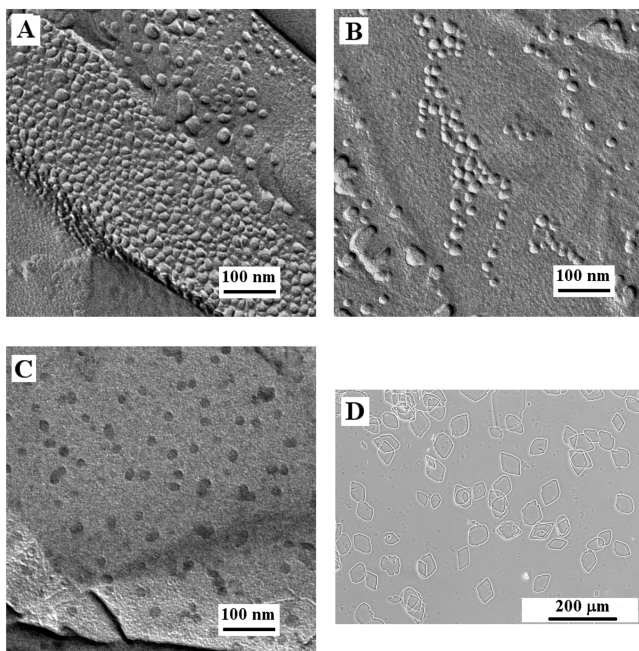


Figure 7. FFEM images of (A) the 10 wt % sample at 25 °C, (B) the 1 wt % sample at 25 °C, and (C) the 1 wt % sample after incubation at 0 °C for 5 min. (D) Optical micrograph of the 1 wt % sample after incubation at 0 °C for 5 min and at ~3 °C for 24 h.

transforms into a white solidlike state, in accordance with the formation of a crystalline phase (the stable crystalline phase). For the 1 wt % sample, when it was cooled to 0 °C and incubated at this temperature for 5 min, the original clear solution turns into an opalescent dispersion, indicating the change in the morphology of the ordered structures (the metastable crystalline phase forms). If the 1 wt % sample was further incubated at a selected low temperature (~3 °C) for 24 h (the stable crystalline phase forms), then large crystals can be seen at the bottom of the glass vial, and upon shaking, these crystals can easily be seen by the naked eye. It is worth noting that the size of the crystals depends on the incubation time: longer incubation times result in the formation of larger crystals. For example, we could usually observe crystals with sizes of 5–10 μm for 6 h and >50 μm for 24 h. However, the actual size of the crystals depends on many factors and cannot be easily controlled.

To investigate further the structures of the metastable crystalline phase and the stable crystalline phase of the 1 wt % sample, we carried out FFEM and optical microscopy studies for the two phases, respectively. The FFEM result in Figure 7C shows that the metastable crystalline phase has disklike structures, and the optical micrograph in Figure 7D reveals that the stable crystalline phases are quadrilaterally shaped. The FFEM image in Figure 7C also points out that the “disk” is very thin and that the metastable crystalline phase is probably unilamellar because it is formed by the elongation of micelles during the cooling-induced ordering and crystallization. The FFEM image of the disklike metastable phase observed in the

present $C_{16}\text{mimCl}$ system is similar to that observed in the bicelle (bilayered micelle, a typical disk structure) system composed of lipid mixtures.⁵³ Besides, the absence of the periodic Bragg peaks in the SAXS curve for the same sample (Figure S5 and corresponding explanations in the Supporting Information) also proves the unilamellar character of the metastable crystalline phase. The disklike metastable crystalline phase acts as the precursor of the stable crystalline phase, evolving in both the crystal size and the crystal shape to transform finally into the stable crystalline phase.

3.4. Electrical Conductance Measurements. To study the crystallization kinetics of the 1 wt % sample, electrical conductance measurements were performed. The degree of counterion dissociation of the surfactant molecules or micelles can be evaluated by the electrical conductance of the solution, a decrease of which indicates the counterion binding to the surfactant molecules or micelles.⁶ Figure 8 shows the time

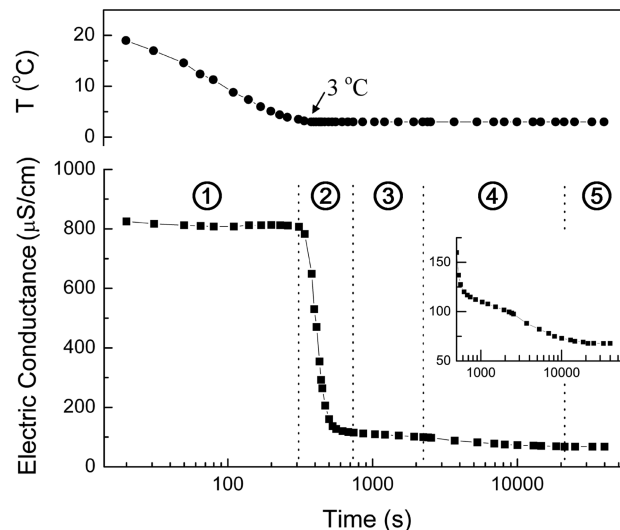


Figure 8. Changes in the electrical conductance of the 1 wt % $C_{16}\text{mimCl}-\text{H}_2\text{O}$ sample after transferring to the 3 °C water bath (lower line). The upper line gives the corresponding temperatures of the sample. The inset gives the magnified figure showing the electrical conductance change after 500 s.

evolution of the electrical conductance of the 1 wt % $C_{16}\text{mimCl}$ solution when the temperature drops from 25 to 3 °C. We can see from the figure that the sample solution reaches the target temperature of 3 °C in about 5 min. During this period (stage 1), although the temperature decreases, the conductance remains almost unchanged, indicating that spherical micelles are reserved. At 5 min, the initial micellar phase starts to convert to the metastable crystalline phase, and a complete conversion takes about 7 min (stage 2). After an induction period (stage 3), the metastable crystalline phase gradually transforms into the stable crystalline phase upon prolonged incubation, and complete conversion takes about 5 h (stage 4). The above results show that the conversion from the fluid micellar phase to the metastable crystalline phase is much faster than the conversion from the metastable crystalline phase to the stable crystalline phase. The conductance values of the fluid micellar phase, metastable crystalline phase, and stable crystalline phase are 816 ± 10 , 110 ± 8 , and $70 \pm 6 \mu\text{S}/\text{cm}$, respectively. The much larger conductance of the micellar phase compared to those of the two crystalline phases indicates

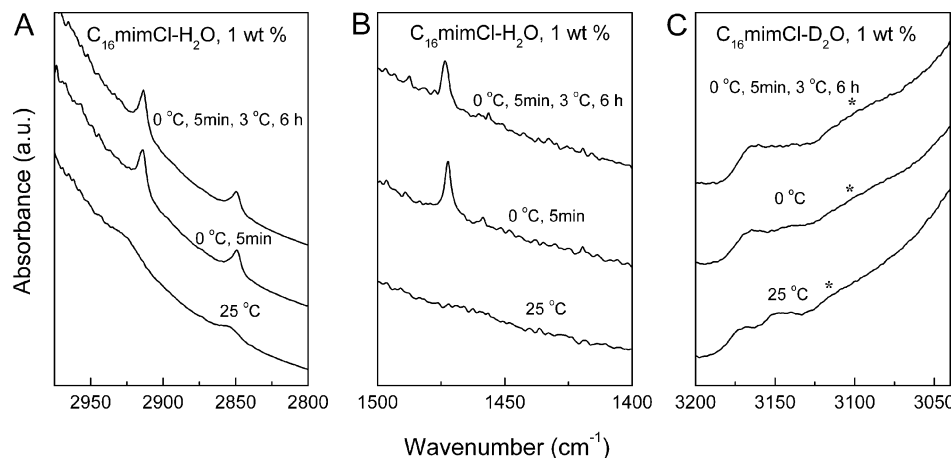


Figure 9. FTIR absorbance spectra of the 1 wt % $C_{16}\text{mimCl}$ aqueous dispersions. (A) $C_{16}\text{mimCl}-\text{H}_2\text{O}$, 2975–2800 cm^{-1} . (B) $C_{16}\text{mimCl}-\text{H}_2\text{O}$, 1500–1400 cm^{-1} . (C) $C_{16}\text{mimCl}-\text{D}_2\text{O}$, 3200–3040 cm^{-1} .

that the surface charge density of the micellar phase is much lower than those of the two crystalline phases. The rationale is as follows.

The decrease in the conductance of the dispersion upon crystallization indicates a reduced concentration of the dissociated counterions (Cl^-) in the bulk solution. This means that the surfaces of the two crystalline phases have a stronger ability to “capture” counterions as compared to that of the spherical micellar phase. As concluded in the literature,^{6–8,54} a membrane with a larger surface charge density has a stronger counterion binding ability (or a weaker counterion release ability). For aggregates composed of the same molecules, the surface charge density is related to the surface curvature of the aggregates: a smaller surface curvature usually has a greater surface charge density. Thus, our electrical conductivity results suggest that the two crystalline phases have a larger membrane surface charge density (resulting from a lower surface curvature) than does the spherical phase, which is related to the tighter packing of the surfactant molecules in the two crystalline phases. The similar conductance values of the two crystalline phases indicate that they are similar in membrane surface curvature and charge density, which can be supported by the flat morphology revealed by our microscopy results in Figure 7. There are two reasons for the lower electrical conductance observed in the stable crystalline phase as compared to that observed in the metastable crystalline phase: (1) The stable crystalline phase is more ordered and more tightly packed than the metastable crystalline phase, consistent with our WAXS results for the 1 wt % sample in Figure 5A,B. (2) In the condensed multilamellar stable crystalline phase, a larger number of counterions are confined within the interlamellar region of the multilamellar crystals and are therefore not able to conduct electricity.

3.5. FTIR. To provide a submolecular understanding of the phase behavior of $C_{16}\text{mimCl}$ aqueous dispersions, we carried out FTIR experiments for the 1 wt % $C_{16}\text{mimCl}$ sample. Shown in Figure 9A,B are the FTIR absorbance spectra of the $C_{16}\text{mimCl}-\text{H}_2\text{O}$ system in the regions of 2975–2800 and 1500–1400 cm^{-1} . In Figure 9A, in the spherical fluid micellar phase at 25 °C, the CH_2 asymmetrical and symmetrical stretching vibrations ($\nu_{as}\text{CH}_2$ and $\nu_s\text{CH}_2$) of the long alkyl chains in the surfactant tail region are broad and centered at 2925.6 and 2854.6 cm^{-1} , respectively, whereas in the metastable crystalline phase (after incubation at 0 °C for 5 min) and the

stable crystalline phase (after incubations at 0 °C for 5 min and at 3 °C for 6 h) the centers of the $\nu_{as}\text{CH}_2$ and $\nu_s\text{CH}_2$ bands shift to ~2914 and ~2850 cm^{-1} , respectively. The downward shifts of the band positions and the sharpening of the bandwidth indicate that the number of trans conformers in the long alkyl chains increases significantly during the fluid micellar-to-crystalline transition.^{55–59} The similar band positions and band widths of the two crystalline phases show that they are almost the same in the alkyl chain conformations. Another important band is the CH_2 scissoring vibration (δCH_2) in the long alkyl chains (Figure 9B), which is very sensitive to the intermolecular forces and can serve as a key band for examining the state of packing of the methylene chains in various phases.^{55–59} At 25 °C in the spherical micellar phase, the very broad, shallow band ranging from 1485 to 1440 cm^{-1} suggests that the long alkyl chains are in the disordered or fused state. In the metastable crystalline phase, a sharp δCH_2 band at 1472.2 cm^{-1} is seen, suggesting that the methylene trans-zigzag planes are packed in an ordered triclinic state. In the stable crystalline phase, the sharp δCH_2 band blue shifts by a small amount to 1473.6 cm^{-1} , indicating that the alkyl chains are in a close-to-triclinic packing state. The higher wavenumber of the stable crystalline phase indicates tighter packing of the hydrocarbon groups in the surfactant tail region, which is consistent with the WAXS result.

To study the hydrogen bonding interaction involving the imidazolium cations of the $C_{16}\text{mimCl}$ molecules, the CH stretching vibrations at positions 2, 4, and 5 on the imidazolium ring ($\nu\text{C}_{(2)}-\text{H}$ and $\nu\text{C}_{(4,5)}-\text{H}$) at 3200–3050 cm^{-1} are frequently used as spectral probes for studying the cation–anion and cation–solvent interactions.^{60–72} However, these bands are very weak in intensity and are severely affected by the strong H_2O absorption in the 3700–3000 cm^{-1} region in our $C_{16}\text{mimCl}-\text{H}_2\text{O}$ samples (data not shown). Thus, the $C_{16}\text{mimCl}-\text{D}_2\text{O}$ samples were used instead to improve the spectral quality. Because the DSC results of the 1 wt % $C_{16}\text{mimCl}-\text{D}_2\text{O}$ samples (data not shown) are very similar to those of the 1 wt % $C_{16}\text{mimCl}-\text{H}_2\text{O}$ samples, it is reasonable to interpret the IR results on the basis of the $C_{16}\text{mimCl}-\text{D}_2\text{O}$ systems. In Figure 9C, the 3200–3040 cm^{-1} region contains roughly two absorption regions; the one at 3190–3125 cm^{-1} is assigned to $\nu\text{C}_{(4,5)}-\text{H}$, and the other at 3125–3060 cm^{-1} is assigned to $\nu\text{C}_{(2)}-\text{H}$.^{62,65} During the fluid micellar (25 °C) to metastable crystalline (0 °C) transition, large changes in the

band shapes and band positions can be seen for $\nu C_{(4,5)}-H$ and $\nu C_{(2)}-H$, indicating the changes in the conformation and hydration of the polar imidazolium cation.

Because it has been reported that the most favorable site for an imidazolium cation to H bond to an anion or a solvent molecule is $C_{(2)}-H$,^{60–64,66–72} this means that the $\nu C_{(2)}-H$ band is sensitive to the change in the hydrogen bonding strength of the imidazolium cation. The red shift (from ~ 3114 to $\sim 3100\text{ cm}^{-1}$) of the band position during the micellar ($25\text{ }^\circ\text{C}$) to metastable crystalline ($0\text{ }^\circ\text{C}$) phase transition suggests an increase in the hydrogen bonding strength between the $C_{(2)}-H$ in the ring and the hydrogen bond acceptors. According to previous surveys,^{66,71,72} the hydrogen bonding interaction between the imidazolium cation and counterion (which is a charge-enhanced hydrogen bonding interaction) is stronger than that between the imidazolium cation and water. Thus, the increase in the hydrogen bonding strength during the crystallization process indicates a partial dehydration of the imidazolium cation. Thus, the large red shift ($\sim 14\text{ cm}^{-1}$) in the $\nu C_{(2)}-H$ band position during the fluid micellar to metastable crystalline transition suggests a significant dehydration of the imidazolium cation. During the metastable crystalline to stable crystalline phase transition, the small change in the band shape of $\nu C_{(4,5)}-H$ indicates a small change in the vibrational environment of $C_{(4,5)}-H$, and the similar (or perhaps a slight red shift) band position of $\nu C_{(2)}-H$ indicates a similar degree of hydration (or a slight decrease in the degree of hydration) of the polar imidazolium cation in the two crystalline phases.

In summary, the above IR results indicate that during the micellar to metastable crystalline phase transition large rearrangements occur in the conformation and hydration of the imidazolium head region and in the conformation and packing states of the alkyl tail region. During the metastable crystalline to stable crystalline phase transition, a small change in the conformation and/or hydration in the head and a notable change in the packing state of the alkyl tail take place.

3.6. Formation and Transformation of Two Crystalline Phases.

We recently reported the phase behavior of $C_{16}\text{mimCl}$ aqueous dispersions in the high-concentration region (10 – 67 wt \%).¹¹ It was found that at 10 – 25 wt \% the samples change directly from a spherical micellar solution to a lamellar crystalline phase upon cooling. At higher concentrations (50 and 67 wt \%), a hexagonal micellar phase forms at temperatures of around $30\text{ }^\circ\text{C}$ during heating, and upon cooling, it first converts to a lamellar gel phase and then to a lamellar crystalline phase.

The stable crystalline phases in the 1 and 10 wt \% samples in this work exhibit the same WAXS peaks as those in the crystalline phases of the 10 – 67 wt \% samples.¹¹ Besides, they have the same lamellar repeat distance (3.2 nm) and the same crystalline to micellar transition enthalpy ($\sim 55\text{ kJ/mol}$) upon heating. These facts mean that the crystalline phase in our previous work is the stable crystalline form. The alkyl tails of the stable crystalline phase were supposed to adopt a tilted and/or interdigitated packing state.¹¹

Our present work demonstrates that the metastable crystalline phase prefers to form at dilute concentrations (1 wt \% or lower) whereas the stable crystalline phase forms more easily at higher concentrations. In dilute samples, the metastable crystalline phase first occurs as the temperature decreases to below $2\text{ }^\circ\text{C}$, and upon prolonged incubation at $3\text{ }^\circ\text{C}$, it eventually converts to the stable crystalline phase. As revealed by WAXS and FTIR, the two crystalline phases have

different packing states of the alkyl tail and a small difference in the headgroup conformation and/or hydration.

The formation of two crystalline phases was also reported for a pyridinium-based surfactant, cetylpyridinium chloride (CPC), in aqueous solutions.^{6–8} The only difference between CPC and $C_{16}\text{mimCl}$ is the headgroup structure. The largest difference in the phase behaviors of the two surfactant systems lies in the structure of the metastable crystalline phase. The metastable crystalline phase of CPC is multilamellar and needlelike,^{6,7} but that of $C_{16}\text{mimCl}$ is probably unilamellar and disklike. This means that the crystallization mechanisms for the more stable crystalline phase are different for the two systems because they have different intermediate metastable crystalline structures.

To summarize the phase transformations among the spherical fluid micelle, the disklike metastable crystalline phase, and the multilamellar stable crystalline phase, a schematic drawing is illustrated in Figure 10. The formation

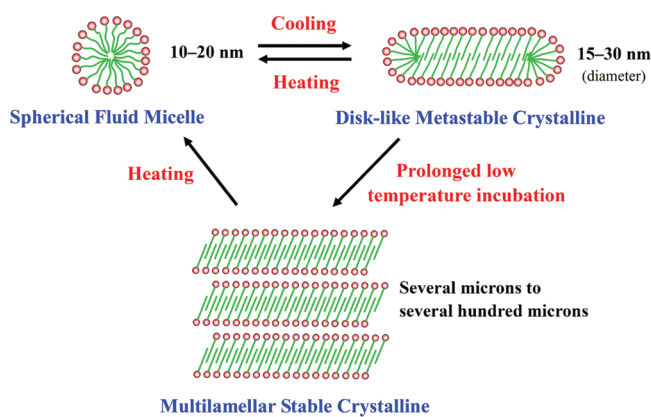


Figure 10. Schematic drawing showing the phase transformations among the fluid micelle, metastable crystalline phase, and stable crystalline phase for 1 wt \% $C_{16}\text{mimCl}$ aqueous dispersions.

of different phases with various morphologies can be explained by the critical packing parameter P_c expressed as $P_c = V/(al)$, where V is the surfactant tail volume, a is the effective headgroup area, and l is the extended length of the alkyl chain, respectively.^{73,74} When $P_c < 1/3$, spherical micelles form. At $1/3 < P_c < 1/2$, cylindrical or rod-shaped micelles form. When P_c approaches 1, lamellar structures form. The relative sizes of the head and tail parts of the $C_{16}\text{mimCl}$ molecules are affected by the hydration and mobility of the head part and by the conformation and packing of the alkyl chain tails. For the 0.5 – 10 wt \% sample at $25\text{ }^\circ\text{C}$, the disordered, loosely packed surfactant tails and the repulsive electrostatic interactions between the positively charged imidazolium groups (incurred by the release of counterions) allow a large space for the headgroup to be well-hydrated. This leads to a P_c value of $< 1/3$, and thus spherical micelles form. At low temperature (below $5\text{ }^\circ\text{C}$ for the 10 wt \% sample and below $2\text{ }^\circ\text{C}$ for the 1 wt \% sample), the separation between the imidazolium groups is restricted by the ordered and tightly packed alkyl tails. This increases the surface charge density and thus enhances the counterion binding ability, which further lowers the hydration and mobility of the polar heads. The significant decrease in the degree of hydration and the mobility of the head part largely decreases a , which makes P_c approach 1, leading to the formation of lamellar structures.

The present work gives a detailed submolecular characterization of the phase transformation processes of imidazolium-based cationic surfactant C₁₆mimCl. Knowledge about such submolecular information of surfactants can set the foundation for the modulation of the formation kinetics or even the formation pathway of the desired crystalline materials. A deeper understanding of the crystallization pathway enables us to optimize the experimental conditions to produce single crystals of surfactants large enough for X-ray structural analysis. Moreover, because many surfactant molecules are insolubilized and even solidified with decreasing temperature of their aqueous solutions,^{7,8} this work may also have implications for the purification of surfactants.

4. CONCLUSIONS

We have studied the self-assembly and phase behavior of C₁₆mimCl aqueous dispersions. Particular efforts have been devoted to investigating the formation and transformation of the two crystalline phases. At higher concentrations (e.g., 10 wt %), the initial fluid spherical micellar phase directly converts to the stable multilamellar crystalline phase upon cooling. However, at lower concentrations (e.g., 1 wt %), the micelles first convert to a metastable crystalline phase, which subsequently transforms to the stable crystalline phase upon prolonged low-temperature incubation.

The most interesting result is that the disklike metastable crystalline phase can be regarded as the prestructure of the stable multilamellar platelike crystalline phase. Actually, our WAXS, FFEM, electrical conductance, and FTIR data all support the above conclusion. In particular, the FTIR results provide a submolecular-level picture of the stepwise ordering of the cooling-induced crystallization process of C₁₆mimCl, showing that large rearrangements occur in the conformation and hydration of the imidazolium head and in the conformation and packing states of the alkyl tail during the micellar to metastable crystalline phase transition. During the metastable crystalline to stable crystalline phase transition, a small change in the conformation and/or hydration in the head and a notable change in the packing state of the alkyl tail happen. Because the crystallization process is very common in both surfactants and ionic liquids, the formation of a preordered structure prior to the final crystalline state deepens our understanding of the crystallization mechanisms of these substances and should thus be widely recognized and explored.

■ ASSOCIATED CONTENT

S Supporting Information

ITC titration curve, DSC results for the 0.5–10 wt % C₁₆mimCl solutions, and additional XRD data. This material is available free of charge via the Internet at <http://pubs.acs.org>.

■ AUTHOR INFORMATION

Corresponding Author

*Tel: (+86)10 6279 2492. Fax: (+86)10 6277 1149. E-mail: yuzhw@tsinghua.edu.cn.

Notes

The authors declare no competing financial interest.

■ ACKNOWLEDGMENTS

This work was supported by grants from the Natural Science Foundation of China (grant nos. 20973100 and 21133009). The SAXS and WAXS data were collected at beamline 1W2A

of the Beijing Synchrotron Radiation Facility (BSRF) with the assistance of Dr. Zhong-Hua Wu and Guang Mo.

■ REFERENCES

- (1) Behnke, G.; Bilz, H.; Buettner, H. Polymorphism of Silica and Ice. *Phys. Rev. Lett.* **1986**, *56*, 1276.
- (2) Guillou, N.; Louër, M.; Auffrédic, J. P.; Louër, D. Two Polymorphic Forms of Ceric Potassium Nitrate, K₂Ce(NO₃)₆. *Acta Crystallogr., C* **1995**, *51*, 1029.
- (3) Dunitz, J. D.; Bernstein, J. Disappearing Polymorphs. *Acc. Chem. Res.* **1995**, *28*, 193.
- (4) Caira, M. R. Crystalline Polymorphism of Organic Compounds. *Top. Curr. Chem.* **1998**, *198*, 163.
- (5) Braga, D.; Grepioni, F.; Maini, L.; Polito, M. Crystal Polymorphism and Multiple Crystal Forms. *Struct. Bonding (Berlin)* **2009**, *132*, 25.
- (6) Sasaki, S. Metastable Crystalline Lamella of Cetylpyridinium Chloride in the Krafft Transition. *J. Phys. Chem. B* **2007**, *111*, 2473.
- (7) Sasaki, S. Kinetic Studies on Hydrated Solid Transform of Cetylpyridinium Chloride in Aqueous Solution. *J. Phys. Chem. B* **2009**, *113*, 8545.
- (8) Sasaki, S. Transformation Relationships among Monomers, Micelles, Metastable Solid, and Stable Solid in Aqueous Cetylpyridinium Chloride Solution. *J. Phys. Chem. B* **2010**, *114*, 11039.
- (9) Wu, F. G.; Chen, L.; Yu, Z. W. Water Mediates the Metastable Crystal-to-Stable Crystal Phase Transition Process in Phospholipid Aqueous Dispersion. *J. Phys. Chem. B* **2009**, *113*, 869.
- (10) Wu, F. G.; Yu, Z. W.; Ji, G. Formation and Transformation of the Subgel Phase in Dioctadecyldimethylammonium Bromide Aqueous Dispersions. *Langmuir* **2011**, *27*, 2349.
- (11) Wu, F. G.; Wang, N. N.; Zhang, Q. G.; Sun, S. F.; Yu, Z. W. Crystallization from the Micellar Phase of Imidazolium-Based Cationic Surfactants. *J. Colloid Interface Sci.* **2012**, *374*, 197.
- (12) Mahmoudi, G.; Morsali, A. Crystal-to-Crystal Transformation from a Weak Hydrogen-Bonded Two-Dimensional Network Structure to a Two-Dimensional Coordination Polymer on Heating. *Cryst. Growth Des.* **2008**, *8*, 391.
- (13) Ghosh, A. K.; Woo, E. M.; Sun, Y. S.; Lee, L. T.; Wu, M. C. Characterization and Analyses on Complex Melting, Polymorphism, and Crystal Phases in Melt-Crystallized Poly(hexamethylene terephthalate). *Macromolecules* **2005**, *38*, 4780.
- (14) Zhu, B.; Kai, W. H.; Pan, P. J.; Yazawa, K.; Nishida, H.; Sakurai, M.; Inoue, Y. Polymorphic Packing and Dynamics of Biodegradable Poly(3-hydroxypropionate). *J. Phys. Chem. B* **2008**, *112*, 9684.
- (15) Ostwald, W. Studies on the Formation and Transformation of Solid Materials. *Z. Phys. Chem. (Leipzig)* **1897**, *22*, 289.
- (16) Li, L. B.; Groenewold, J.; Picken, S. J. Transient Phase-Induced Nucleation in Ionic Liquid Crystals and Size-Frustrated Thickening. *Chem. Mater.* **2005**, *17*, 250.
- (17) Unger, G.; Zheng, X. B. Learning Polymer Crystallization with the Aid of Linear, Branched and Cyclic Model Compounds. *Chem. Rev.* **2001**, *101*, 4157.
- (18) Li, L. B.; de Jeu, W. H. Shear-Induced Smectic Ordering as a Precursor of Crystallization in Isotactic Polypropylene. *Macromolecules* **2003**, *36*, 4862.
- (19) Li, L. B.; de Jeu, W. H. Shear-Induced Smectic Ordering in the Melt of Isotactic Polypropylene. *Phys. Rev. Lett.* **2004**, *92*, 075506.
- (20) Stoppa, A.; Zech, O.; Kunz, W.; Buchner, R. The Conductivity of Imidazolium-Based Ionic Liquids from (−35 to 195) °C. A Variation of Cation's Alkyl Chain. *J. Chem. Eng. Data* **2010**, *55*, 1768.
- (21) Zech, O.; Stoppa, A.; Buchner, R.; Kunz, W. The Conductivity of Imidazolium-Based Ionic Liquids from (248 to 468) K. B. Variation of the Anion. *J. Chem. Eng. Data* **2010**, *55*, 1774.
- (22) Holbrey, J. D.; Seddon, K. R. The Phase Behaviour of 1-Alkyl-3-methylimidazolium Tetrafluoroborates; Ionic Liquids and Ionic Liquid Crystals. *J. Chem. Soc., Dalton Trans.* **1999**, *13*, 2133.
- (23) Bradley, A. E.; Hardacre, C.; Holbrey, J. D.; Johnston, S.; McMath, S. E. J.; Nieuwenhuyzen, M. Small-Angle X-ray Scattering

- Studies of Liquid Crystalline 1-Alkyl-3-methylimidazolium Salts. *Chem. Mater.* **2002**, *14*, 629.
- (24) Blesic, M.; Swadźba-Kwaśny, M.; Belhocine, T.; Gunaratne, H. Q. N.; Canongia Lopes, J. N.; Gomes, M. F. C.; Padua, A. A. H.; Seddon, K. R.; Rebelo, L. P. N. 1-Alkyl-3-methylimidazolium Alkanesulfonate Ionic Liquids, $[C_nH_{2n+1}mim][C_kH_{2k+1}SO_3]$: Synthesis and Physicochemical Properties. *Phys. Chem. Chem. Phys.* **2009**, *11*, 8939.
- (25) Tariq, M.; Serro, A. P.; Mata, J. L.; Saramago, B.; Esperanca, J. M. S. S.; Canongia Lopes, J. N.; Rebelo, L. P. N. High-Temperature Surface Tension and Density Measurements of 1-Alkyl-3-methylimidazolium Bistriflamide Ionic Liquids. *Fluid Phase Equilib.* **2010**, *294*, 131.
- (26) Eastoe, J.; Gold, S.; Rogers, S. E.; Paul, A.; Welton, T.; Heenan, R. K.; Grillo, I. Ionic Liquid-in-Oil Microemulsions. *J. Am. Chem. Soc.* **2005**, *127*, 7302.
- (27) Zech, O.; Thomaier, S.; Bauduin, P.; Rück, T.; Touraud, D.; Kunz, W. Microemulsions with an Ionic Liquid Surfactant and Room Temperature Ionic Liquids as Polar Pseudo-Phase. *J. Phys. Chem. B* **2009**, *113*, 465.
- (28) Harrar, A.; Zech, O.; Klaus, A.; Bauduin, P.; Kunz, W. Influence of Surfactant Amphiphilicity on the Phase Behavior of IL-Based Microemulsions. *J. Colloid Interface Sci.* **2011**, *362*, 423.
- (29) Harrar, A.; Zech, O.; Hartl, R.; Bauduin, P.; Zemb, T.; Kunz, W. $[emim][etSO_4]$ as the Polar Phase in Low-Temperature-Stable Microemulsions. *Langmuir* **2011**, *27*, 1635.
- (30) Zech, O.; Kunz, W. Conditions for and Characteristics of Nonaqueous Micellar Solutions and Microemulsions with Ionic Liquids. *Soft Matter* **2011**, *7*, 5507.
- (31) Gao, Y. A.; Han, S. B.; Han, B. X.; Li, G. Z.; Shen, D.; Li, Z. H.; Du, J. M.; Hou, W. G.; Zhang, G. Y. TX-100/Water/1-Butyl-3-methylimidazolium Hexafluorophosphate Microemulsions. *Langmuir* **2005**, *21*, 5681.
- (32) Gao, Y. A.; Li, N.; Zheng, L. Q.; Zhao, X. Y.; Zhang, S. H.; Han, B. X.; Hou, W. G.; Li, G. Z. A Cyclic Voltammetric Technique for the Detection of Micro-Regions of $bmimPF_6/Tween\ 20/H_2O$ Microemulsions and Their Performance Characterization by UV-Vis Spectroscopy. *Green Chem.* **2006**, *8*, 43.
- (33) Bowers, J.; Butts, C. P.; Martin, P. J.; Vergara-Gutierrez, M. C.; Heenan, R. K. Aggregation Behavior of Aqueous Solutions of Ionic Liquids. *Langmuir* **2004**, *20*, 2191.
- (34) Goodchild, I.; Collier, L.; Millar, S. L.; Prokeš, I.; Lord, J. C. D.; Butts, C. P.; Bowers, J.; Webster, J. R. P.; Heenan, R. K. Structural Studies of the Phase, Aggregation and Surface Behaviour of 1-Alkyl-3-methylimidazolium Halide + Water Mixtures. *J. Colloid Interface Sci.* **2007**, *307*, 455.
- (35) Blesic, M.; Marques, M. H.; Plechkova, N. V.; Seddon, K. R.; Rebelo, L. P. N.; Lopes, A. Self-Aggregation of Ionic Liquids: Micelle Formation in Aqueous Solution. *Green Chem.* **2007**, *9*, 481.
- (36) Blesic, M.; Swadźba-Kwaśny, M.; Holbrey, J. D.; Canongia Lopes, J. N.; Seddon, K. R.; Rebelo, L. P. N. New Cationic Surfactants Based on 1-Alkyl-3-methylimidazolium Alkylsulfonates, $[C_nH_{2n+1}mim][C_mH_{2m+1}SO_3]$: Mesomorphism and Aggregation. *Phys. Chem. Chem. Phys.* **2009**, *11*, 4260.
- (37) Dong, B.; Li, N.; Zheng, L. Q.; Yu, L.; Inoue, T. Surface Adsorption and Micelle Formation of Surface Active Ionic Liquids in Aqueous Solution. *Langmuir* **2007**, *23*, 4178.
- (38) Dong, B.; Zhao, X. Y.; Zheng, L. Q.; Zhang, J.; Li, N.; Inoue, T. Aggregation Behavior of Long-Chain Imidazolium Ionic Liquids in Aqueous Solution: Micellization and Characterization of Micelle Microenvironment. *Colloids Surf., A* **2008**, *317*, 666.
- (39) Dong, B.; Zhang, J.; Zheng, L. Q.; Wang, S. Q.; Li, X. W.; Inoue, T. Salt-Induced Viscoelastic Wormlike Micelles Formed in Surface Active Ionic Liquid Aqueous Solution. *J. Colloid Interface Sci.* **2008**, *319*, 338.
- (40) Vanyúr, R.; Biczók, L.; Miskolczy, Z. Micelle Formation of 1-Alkyl-3-methylimidazolium Bromide Ionic Liquids in Aqueous Solution. *Colloids Surf., A* **2007**, *299*, 256.
- (41) Modaressi, A.; Sifaoui, H.; Mielcarz, M.; Domańska, U.; Rogalski, M. Influence of the Molecular Structure on the Aggregation of Imidazolium Ionic Liquids in Aqueous Solutions. *Colloids Surf., A* **2007**, *302*, 181.
- (42) Singh, T.; Kumar, A. Aggregation Behavior of Ionic Liquids in Aqueous Solutions: Effect of Alkyl Chain Length, Cations, and Anions. *J. Phys. Chem. B* **2007**, *111*, 7843.
- (43) El Seoud, O. A.; Pires, P. A. R.; Abdel-Moghy, T.; Bastos, E. L. Synthesis and Micellar Properties of Surface-Active Ionic Liquids: 1-Alkyl-3-methylimidazolium Chlorides. *J. Colloid Interface Sci.* **2007**, *313*, 296.
- (44) Luczak, J.; Hupka, J.; Thöming, J.; Jungnickel, C. Self-Organization of Imidazolium Ionic Liquids in Aqueous Solution. *Colloids Surf., A* **2008**, *329*, 125.
- (45) Chamiot, B.; Rizzi, C.; Gaillon, L.; Sirieix-Plénet, J.; Lelièvre, J. Redox-Switched Amphiphilic Ionic Liquid Behavior in Aqueous Solution. *Langmuir* **2009**, *25*, 1311.
- (46) Lin, Y. Y.; Qiao, Y.; Yan, Y.; Huang, J. B. Thermo-Responsive Viscoelastic Wormlike Micelle to Elastic Hydrogel Transition in Dual-Component Systems. *Soft Matter* **2009**, *5*, 3047.
- (47) Firestone, M. A.; Dzieława, J. A.; Zapol, P.; Curtiss, L. A.; Seifert, S.; Dietz, M. L. Lyotropic Liquid-Crystalline Gel Formation in a Room-Temperature Ionic Liquid. *Langmuir* **2002**, *18*, 7258.
- (48) Inoue, T.; Dong, B.; Zheng, L. Q. Phase Behavior of Binary Mixture of 1-Dodecyl-3-methylimidazolium Bromide and Water Revealed by Differential Scanning Calorimetry and Polarized Optical Microscopy. *J. Colloid Interface Sci.* **2007**, *307*, 578.
- (49) The peak assigned to the form factor of individual micelles mainly comes from the counterions, and it is much smaller for chloride-containing surfactants relative to that for bromide-containing surfactants. For details, see the following reference: Small-Angle Scattering from Micellar Solutions. *BARC Newsletter*; Founder's Day Special Issue, pp 37–42. <http://www.barc.gov.in/publications/nl/2003/200310-4.pdf>
- (50) Kastantin, M.; Ananthanarayanan, B.; Karmali, P.; Ruoslahti, E.; Tirrell, M. Effect of the Lipid Chain Melting Transition on the Stability of DSPE-PEG(2000) Micelles. *Langmuir* **2009**, *25*, 7279.
- (51) Wu, F. G.; Jia, Q.; Wu, R. G.; Yu, Z. W. Regional Cooperativity in the Phase Transitions of Dipalmitoylphosphatidylcholine Bilayers: The Lipid Tail Triggers the Isothermal Crystallization Process. *J. Phys. Chem. B* **2011**, *115*, 8559.
- (52) Wu, F. G.; Yu, J. S.; Sun, S. F.; Yu, Z. W. Comparative Studies on the Crystalline to Fluid Phase Transitions of Two Equimolar Cationic/Anionic Surfactant Mixtures Containing Dodecylsulfonate and Dodecylsulfate. *Langmuir* **2011**, *27*, 14740.
- (53) Arnold, A.; Labrot, T.; Oda, R.; Dufourc, E. J. Cation Modulation of Bicelle Size and Magnetic Alignment as Revealed by Solid-State NMR and Electron Microscopy. *Biophys. J.* **2002**, *83*, 2667.
- (54) Sasaki, S. Thermally Changing Lattice Distance of Lamella in the Hydrated Solid of Octadecyltrimethylammonium Chloride. *J. Phys. Chem. B* **2008**, *112*, 8586.
- (55) Lewis, R. N. A. H.; McElhaney, R. N. Fourier Transform Infrared Spectroscopy in the Study of Lipid Phase Transitions in Model and Biological Membranes. In *Methods in Molecular Biology*; Dopico, A. M., Ed.; Humana Press: Totowa, NJ, 2007; Vol. 400, p 207.
- (56) Wu, F. G.; Wang, N. N.; Yu, Z. W. Nonsynchronous Change in the Head and Tail of Dioctadecyldimethylammonium Bromide Molecules during the Liquid Crystalline to Coagel Phase Transformation Process. *Langmuir* **2009**, *25*, 13394.
- (57) Wu, F. G.; Luo, J. J.; Yu, Z. W. Infrared Spectroscopy Reveals the Nonsynchronicity Phenomenon in the Glassy to Fluid Micellar Transition of DSPE-PEG2000 Aqueous Dispersions. *Langmuir* **2010**, *26*, 12777.
- (58) Wu, F. G.; Wang, N. N.; Yu, J. S.; Luo, J. J.; Yu, Z. W. Nonsynchronicity Phenomenon Observed during the Lamellar-Micellar Phase Transitions of 1-Stearoyllysophosphatidylcholine Dispersed in Water. *J. Phys. Chem. B* **2010**, *114*, 2158.
- (59) Wu, F. G.; Wang, N. N.; Tao, L. F.; Yu, Z. W. Acetonitrile Induces Nonsynchronous Interdigitation and Dehydration of

Dipalmitoylphosphatidylcholine Bilayers. *J. Phys. Chem. B* **2010**, *114*, 12685.

(60) Tubbs, J. D.; Hoffmann, M. M. Ion-Pair Formation of the Ionic Liquid 1-Ethyl-3-methylimidazolium Bis(triflyl)imide in Low Dielectric Media. *J. Solution Chem.* **2004**, *33*, 381.

(61) Köddermann, T.; Wertz, C.; Heintz, A.; Ludwig, R. The Association of Water in Ionic Liquids: A Reliable Measure of Polarity. *Angew. Chem., Int. Ed.* **2006**, *45*, 3697.

(62) Köddermann, T.; Wertz, C.; Heintz, A.; Ludwig, R. Ion-Pair Formation in the Ionic Liquid 1-Ethyl-3-methylimidazolium Bis(triflyl)imide as a Function of Temperature and Concentration. *ChemPhysChem* **2006**, *7*, 1944.

(63) Yokoczki, A.; Kasprzak, D. J.; Shiflett, M. B. Thermal Effect on C–H Stretching Vibrations of the Imidazolium Ring in Ionic Liquids. *Phys. Chem. Chem. Phys.* **2007**, *9*, 5018.

(64) Wulf, A.; Fumino, K.; Michalik, D.; Ludwig, R. IR and NMR Properties of Ionic Liquids: Do They Tell Us the Same Thing? *ChemPhysChem* **2007**, *8*, 2265.

(65) Kiefer, J.; Fries, J.; Leipertz, A. Experimental Vibrational Study of Imidazolium-Based Ionic Liquids: Raman and Infrared Spectra of 1-Ethyl-3-methylimidazolium Bis(trifluoromethylsulfonyl)imide and 1-Ethyl-3-methylimidazolium Ethylsulfate. *Appl. Spectrosc.* **2007**, *61*, 1306.

(66) Zhang, L. Q.; Xu, Z.; Wang, Y.; Li, H. R. Prediction of the Solvation and Structural Properties of Ionic Liquids in Water by Two-Dimensional Correlation Spectroscopy. *J. Phys. Chem. B* **2008**, *112*, 6411.

(67) Fumino, K.; Wulf, A.; Ludwig, R. The Cation–Anion Interaction in Ionic Liquids Probed by Far-Infrared Spectroscopy. *Angew. Chem., Int. Ed.* **2008**, *47*, 3830.

(68) Fumino, K.; Wulf, A.; Ludwig, R. Strong, Localized, and Directional Hydrogen Bonds Fluidize Ionic Liquids. *Angew. Chem., Int. Ed.* **2008**, *47*, 8731.

(69) Fumino, K.; Wulf, A.; Ludwig, R. The Potential Role of Hydrogen Bonding in Aprotic and Protic Ionic Liquids. *Phys. Chem. Chem. Phys.* **2009**, *11*, 8790.

(70) Wulf, A.; Fumino, K.; Ludwig, R. Comment on “New Interpretation of the CH Stretching Vibrations in Imidazolium-Based Ionic Liquids”. *J. Phys. Chem. A* **2010**, *114*, 685.

(71) Zhang, Q. G.; Wang, N. N.; Yu, Z. W. The Hydrogen Bonding Interactions between the Ionic Liquid 1-Ethyl-3-Methylimidazolium Ethyl Sulfate and Water. *J. Phys. Chem. B* **2010**, *114*, 4747.

(72) Wang, N. N.; Zhang, Q. G.; Wu, F. G.; Li, Q. Z.; Yu, Z. W. Hydrogen Bonding Interactions between a Representative Pyridinium-Based Ionic Liquid $[\text{BuPy}][\text{BF}_4]$ and Water/Dimethyl Sulfoxide. *J. Phys. Chem. B* **2010**, *114*, 8689.

(73) Israelachvili, J. N.; Mitchell, D. J.; Ninham, B. W. Theory of Self-Assembly of Hydrocarbon Amphiphiles into Micelles and Bilayers. *J. Chem. Soc., Faraday Trans. II* **1976**, *72*, 1525.

(74) Tanford, C. Micelle Shape and Size. *J. Phys. Chem.* **1972**, *76*, 3020.